The steady and unsteady backwash vortices

By N. MATSUNAGA

Department of Civil Engineering Hydraulics and Soil Mechanics, Kyushu University,
Fukuoka 812, Japan

AND H. HONJI

Research Institute for Applied Mechanics, Kyushu University, Fukuoka 812, Japan

A circulatory flow called a 'backwash vortex' forms under waves running up a sloping bed. The backwash vortex is classified into two types: the 'steady backwash vortex' and the 'unsteady backwash vortex'. The former is a steady streaming formed when $Re_2 < 90$, and the latter an unsteady separated flow formed when $Re_2 > 90$, where Re_2 is a form of Reynolds number. The ratio of the lengthscale of the backwash vortex to the swash length is proportional to $Re_2^{-\frac{1}{2}}$ when $Re_2 \ll 30$, and becomes constant when Re_2 is sufficiently large.

1. Introduction

It is often observed that beach steps form at the boundary between surf and swash zones on the beaches, and sand ripples form on the bottom floor in shallow water under the surf zone. The authors (Matsunaga & Honji 1980a) have shown by laboratory experiments that the 'backwash vortex', which is an unsteady, separated vortical flow, forms at the edge of the swash zone when backwash turns back into an oncoming wave bore. The backwash vortex erodes a movable sand bed and forms a step along the shoreline. This 'backwash step' induces the formation of sand ripples in the offshore direction.

This paper is concerned with the results of an experimental study on the characteristics of the backwash vortex.

2. Experimental methods

Experiments were carried out by using a water tank as illustrated in figure 1. The tank, made of transparent plastic plates, was 180 cm long, 15 cm wide and 20 cm deep. The tank was equipped with a sloping flat bed. The slopes θ of the bed from the horizontal were 8°, 12° and 32°, with flat plates of length 150, 100 and 50 cm respectively. Wave bores climbing up the sloping bed were formed by oscillating a flap-type wave generator with a motor-crank system. The bore did not break. The stroke of the wave generator at a still water-surface level and the angular frequency ω of run-up movement, which was the same as that of the wave generator, ranged from 3 to 8 cm and from 2.0 to 9.4 s^{-1} respectively. Glycerol–water solutions, of which the kinematic viscosity ν ranged from 0.1 to 4.7 cm^2 s^{-1}, were used as working fluids. The measurements of the characteristic length a of induced vortical flows and the swash length l were performed visually during the experiments. The value of a Reynolds number Re_1 defined as $\omega l^2/\nu$ was varied between 1.4×10 and 4.5×10^4.
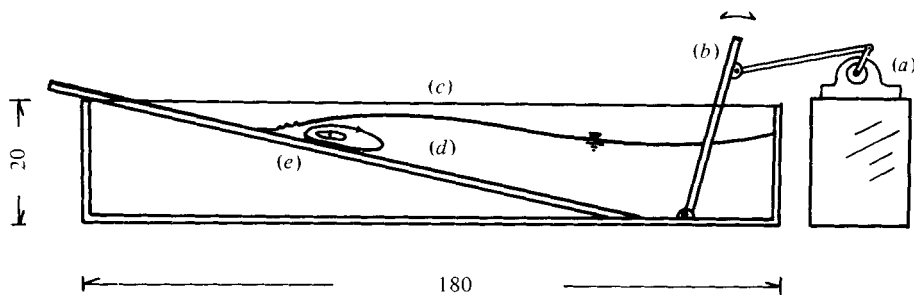
FIGURE 1. Schematic diagram of experimental set-up (dimensions in cm): (a) motor; (b) wave generator; (c) tank; (d) glycerol–water solution; (e) sloping bed.

The direct shadow method (Hagerty & Mich 1950; Kaneko & Honji 1979; Matsunaga & Honji 1980b) was employed to visualize the induced vortical flow patterns. The test section of the tank was illuminated by a nearly parallel beam of intense light through a sidewall of the tank. Two-dimensional flow patterns formed on a white screen put on the back of the other sidewall of the tank were photographed by a 35 mm camera.

## 3. Results and discussion

3.1. *Visualized flow patterns*

Figures 2 (a–f) show the timewise variation of a flow induced by the oscillatory wave motion, T being the time passed from the start of the oscillation. The fluid is at rest in figure 2 (a). Figures 2 (b–d, and f) show flow patterns photographed when backwash has turned back into an oncoming wave bore. Figure 2 (e) shows a flow formed when a wave bore has climbed up along the bed surface. A circulatory flow rotating anticlockwise forms in the cusped region between the sloping bed and the free surface of fluid as shown in figure 2 (b). Figure 2 (c) shows that another circulatory flow rotating clockwise begins to form on the offshore side of the anticlockwise flow. This clockwise flow is considered to be induced by the anticlockwise flow. The circulatory flows shown in figures 2 (d–e) are secondary steady streamings, the flow velocity of which is much smaller than the maximum velocity of the orbital fluid motion due to waves. Since the circulatory flow on the offshore side has the same direction as the backwash vortex due to flow separation as shown by Matsunaga & Honji (1980a), it may be called a 'steady backwash vortex'. The backwash vortex due to flow separation may be called more restrictively an 'unsteady backwash vortex' because the vortex formation by flow separation is time-dependent. In this paper attention is focused on these two types of backwash vortices rather than the anticlockwise flow formed in the cusped region.

The parameters a and l and the two-dimensional polar coordinates (r, ϕ) are defined as in figure 3, where the steady streamings shown in figure 2 are also illustrated; l is the distance between the uppermost point of wave run-up and the lowermost point of wave backwash on the sloping floor. The intersection of the sloping bed and the free surface at rest is chosen as the origin O. The characteristic length a is measured in the r direction from O to the centre of the backwash vortex when a backwash has rushed into an oncoming wave. The quantities l and $1/\omega$ are used as the characteristic lengthscale and timescale respectively of the oncoming waves. The scale a may be expressed as
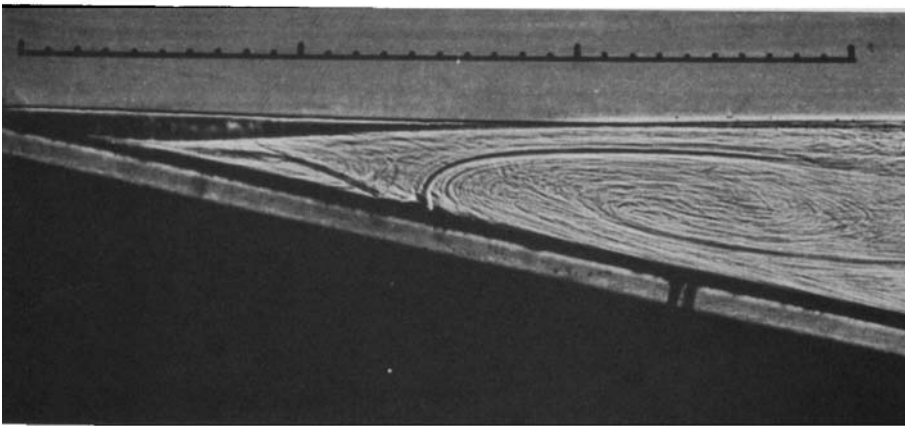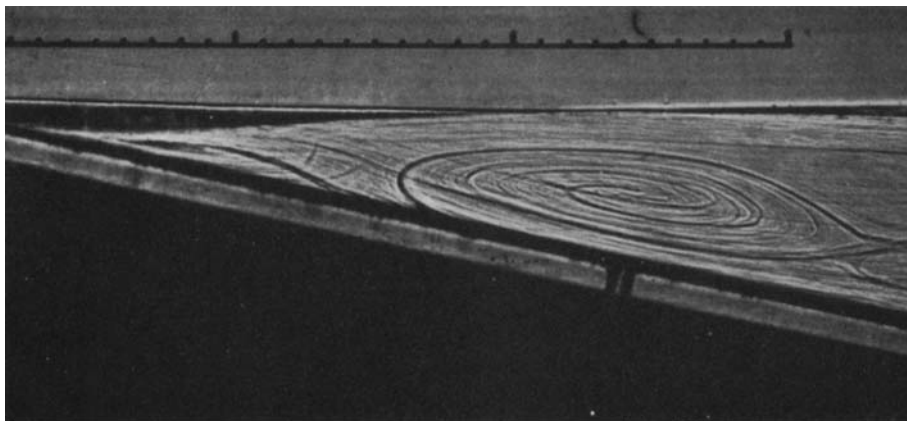
$$a = f(l, \omega, \nu, \theta), \qquad (1)$$
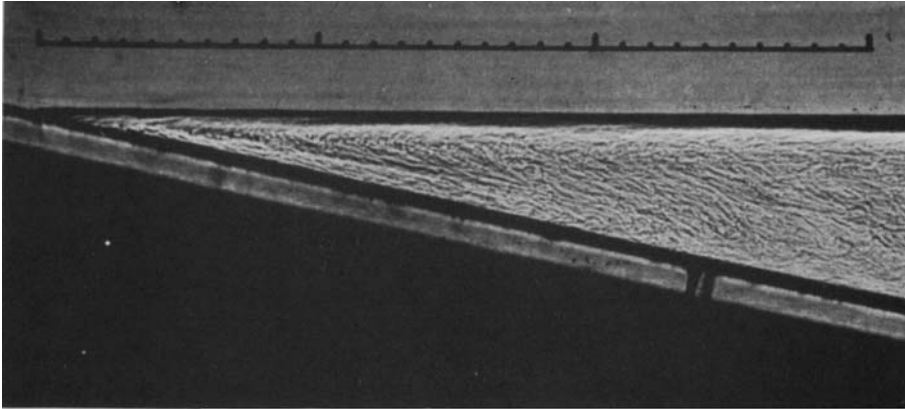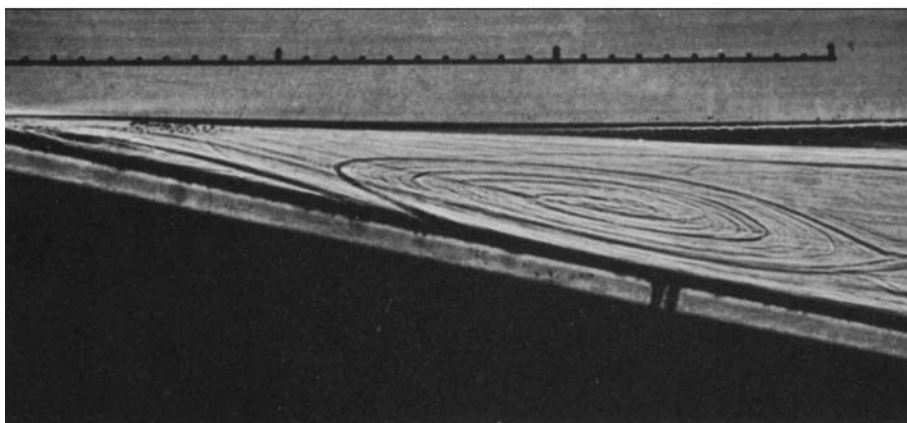
(a)
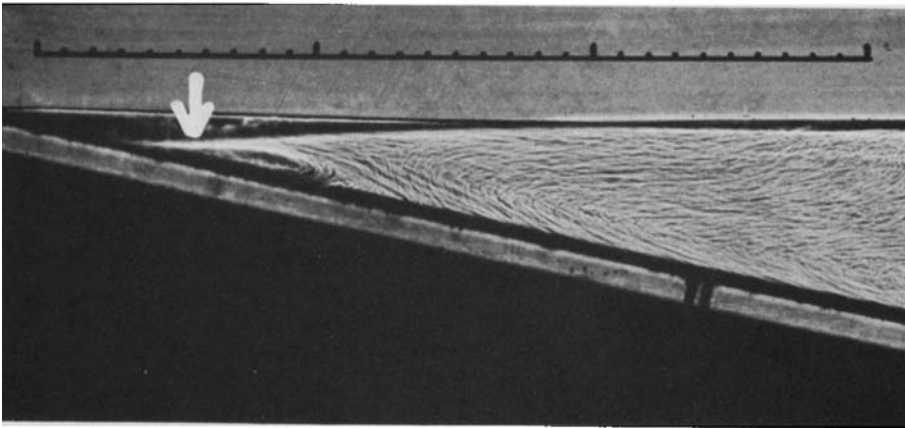
(b)

(c)

FIGURE 2(*a–c*). For caption see p. 192.

FIGURE 2. Development of the standing backwash vortex. Arrow indicates the free surface. Scale unit is cm. $l = 4.5$ cm, $\omega = 4.22$ s^{-1}, $\nu = 3.07$ cm^2 s^{-1}, $\theta = 12°$, $Re_1 = 27.8$. (a) $T = 0$; (b) 0.5 min; (c) 2 min, (d) 6 min; (e) 7 min; (f) 9 min.
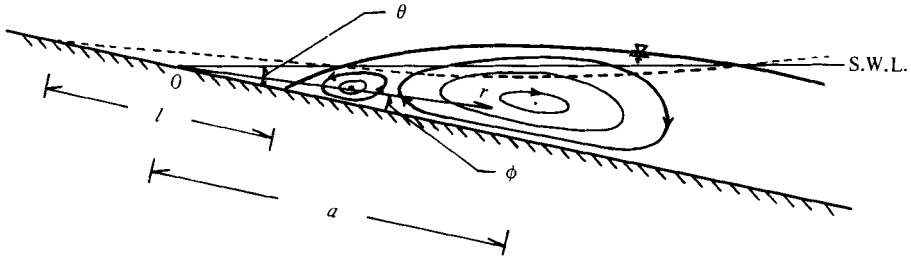
FIGURE 3. Definition of coordinate systems and characteristic quantities on the backwash vortex. Solid line and broken line indicate water surface profiles forming respectively when a backwash has rushed into an oncoming bore and when a bore has climbed along the sloping bed.

and a non-dimensional form of (1) is given by

$$a/l = g(Re_1, \theta), \tag{2}$$

where f and g are functions.

The relationships between a/l and Re_1, and between a/l and θ will be discussed later based on the measured data and flow patterns photographed when the backwash has rushed into an oncoming wave. Figures 4 $(a-c)$ show flow patterns of the backwash vortex when $Re_1 = 1.0 \times 10^2$, 1.0×10^3 and 3.4×10^3 respectively, at $\theta = 12°$. The values of a/l decrease as Re_1 increases. While the flows shown in figures 4 (a, b) are steady backwash vortices, the flow shown in figure 4 (c) is an unsteady backwash vortex because its formation was observed only when a backwash had rushed into an oncoming wave. As will be seen from figure 4, the lengthscale of the anticlockwise-flow region decreases as Re_1 increases. When the unsteady backwash vortex begins to form, the region almost disappears. Through many observations at $\theta = 12°$ by means of the direct shadow method and sawdust method (Matsunaga & Honji 1980a), it has been found that the steady backwash vortex changes gradually into the unsteady one with increase of Re_1, and the critical value of the transition is about $Re_1 = 2.0 \times 10^3$. Figure 5 (a) shows a steady backwash vortex when $\theta = 12°$ and $Re = 510$ and figure 5 (b) when $\theta = 8°$ and $Re_1 = 540$. The values of a/l increase with decrease of θ, though Re_1 are slightly different.

In figure 6 the data for a/l at $\theta = 8°$, $12°$ and $32°$ are plotted against Re_1. The values of a/l are proportional to $Re_1^{-\frac{1}{2}}$ when Re_1 is small, and become constant for large values of Re_1.

3.2. *Relationship between a/l and Reynolds number*

The dependence of a/l on Re_1 may be interpreted as follows. The vortical motion on the sloping bed is described by the vorticity equation for viscous incompressible fluid:
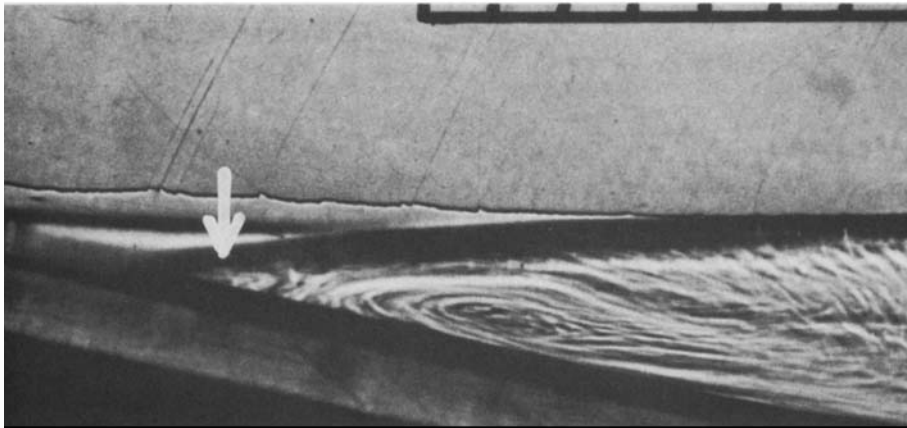
$$\frac{\partial \boldsymbol{\Omega}}{\partial t} - \mathrm{curl}\,(\boldsymbol{u} \times \boldsymbol{\Omega}) = \nu \nabla^2 \boldsymbol{\Omega}, \tag{3}$$

where $\boldsymbol{u}$ is a velocity vector and $\boldsymbol{\Omega} = \mathrm{curl}\,\boldsymbol{u}$ a vorticity vector. For small Reynolds numbers, and possibly also for the lowest Reynolds numbers in the experiments, the motion is dominated by the time-dependent and viscous terms. With $\partial/\partial t \sim 1/\omega$ and $\nabla^2 \sim 1/a^2$, this gives the estimate
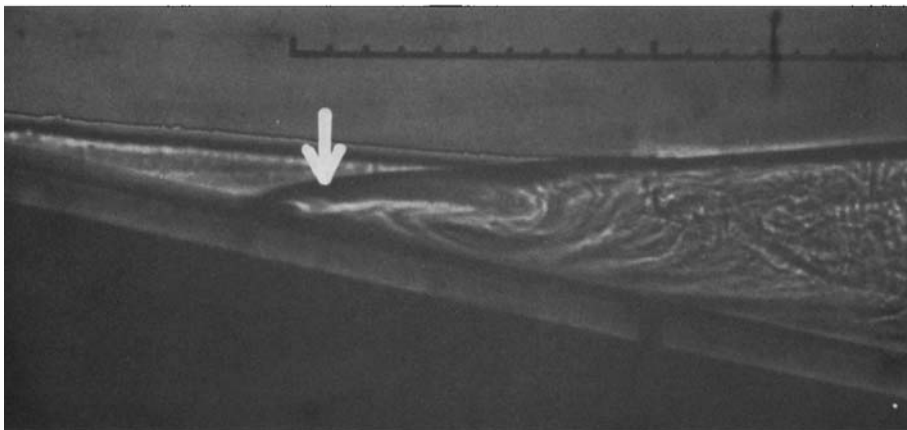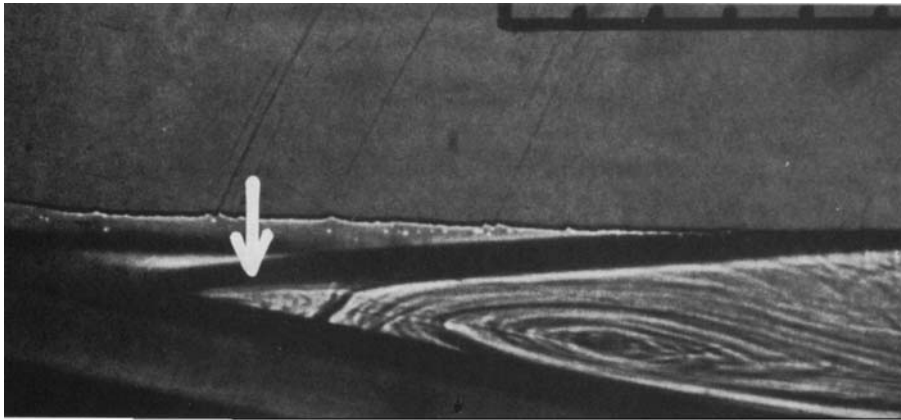
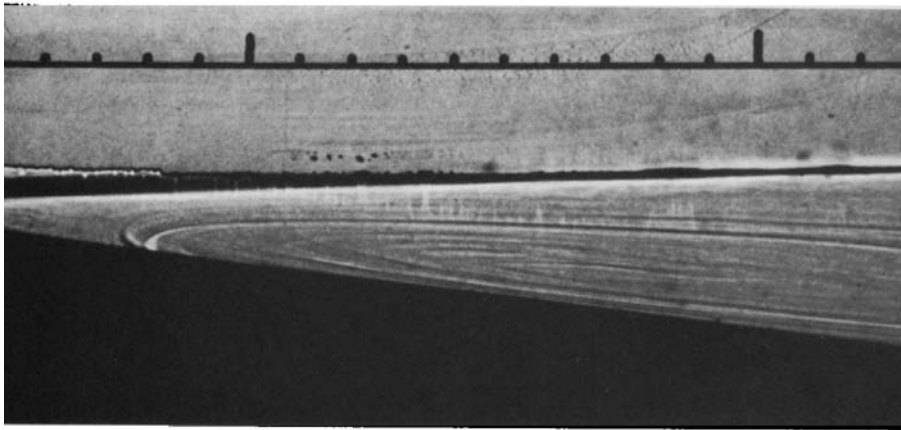$$a \sim (\nu/\omega)^{\frac{1}{2}}. \tag{4}$$
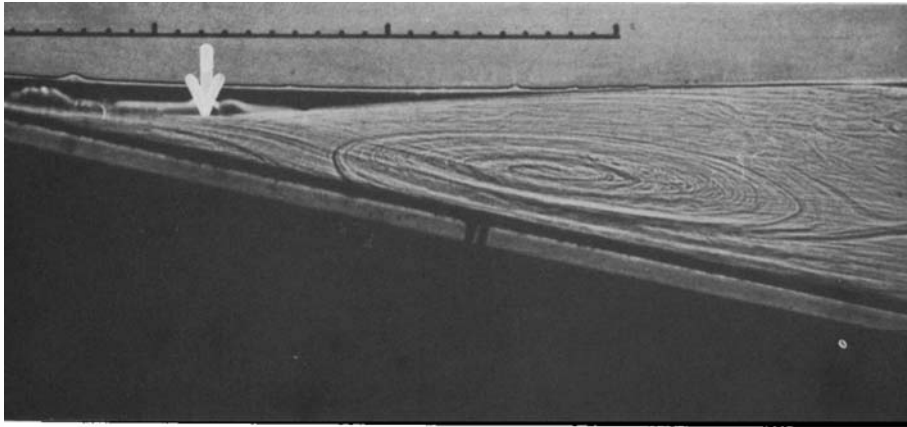
(a)

(b)

(c)

FIGURE 4. Variation of a/l against Re_1 (scale unit in cm). Arrows indicate the free surface. (a) $l = 8.5$ cm, $\omega = 4.22$ s^{-1}, $\nu = 3.00$ cm^2 s^{-1}, $\theta = 12°$, $a = 27.6$ cm, $a/l = 3.25$, $Re_1 = 1.0 \times 10^2$; (b) $l = 8.0$ cm, $\omega = 4.19$ s^{-1}, $\nu = 0.266$ cm^2 s^{-1}, $\theta = 12°$, $a = 7.7$ cm, $a/l = 0.96$, $Re_1 = 1.0 \times 10^3$; (c) $l = 14.9$ cm, $\omega = 3.71$ s^{-1}, $\nu = 0.242$ cm^2 s^{-1}, $\theta = 12°$, $a = 11.2$ cm, $a/l = 0.75$, $Re_1 = 3.4 \times 10^3$.

(a)

(b)

FIGURE 5. Variation of a/l against θ (scale unit in cm). Arrow indicates the free surface. (a) $l = 6.5$ cm, $\omega = 4.19$ s^{-1}, $\nu = 0.344$ cm^2 s^{-1}, $\theta = 12°$, $a = 7.5$ cm, $a/l = 1.15$, $Re_1 = 510$; (b) $l = 8.2$ cm, $\omega = 3.14$ s^{-1}, $\nu = 0.388$ cm^2 s^{-1}, $\theta = 8°$, $a = 21.0$ cm, $a/l = 2.56$, $Re_1 = 540$.

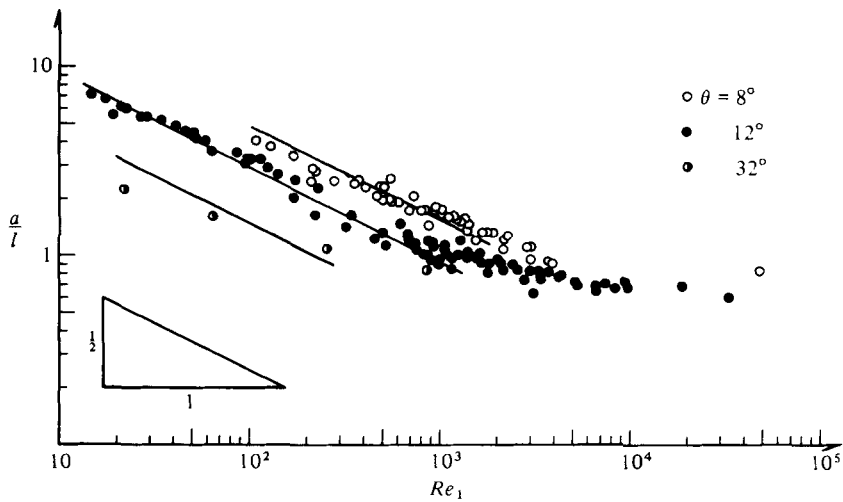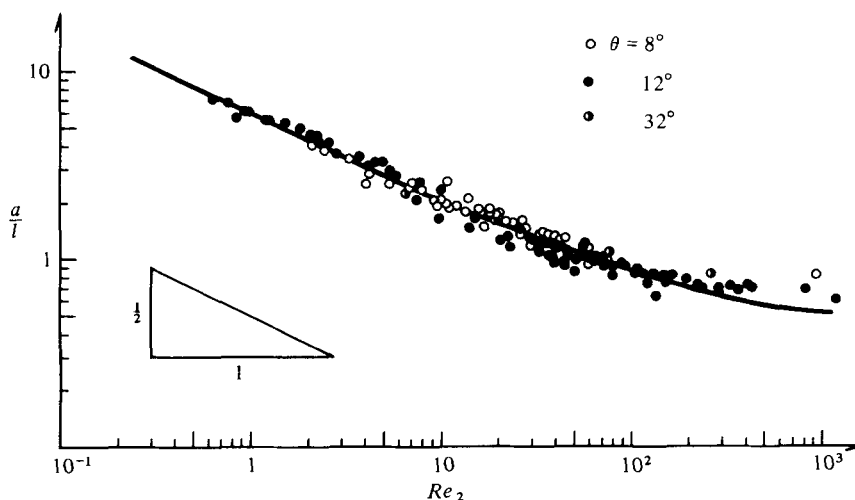FIGURE 6. Re_1 dependence of a/l.

FIGURE 7. Re_2 dependence of a/l.

A non-dimensional form of a is given by

$$\frac{a}{l} \sim \left(\frac{\nu}{\omega l^2}\right)^{\frac{1}{2}} = Re_1^{-\frac{1}{2}}. \tag{5}$$

As the unsteadiness of the driving force increases, the value of a/l becomes smaller and smaller because of the decrease of the thickness of the oscillatory boundary layer, and eventually the steady backwash vortex begins to change into the unsteady one. The lengthscale of the unsteady backwash vortex at larger values of Re_1 may be determined by the relation

$$\frac{\partial \boldsymbol{\Omega}}{\partial t} \sim \text{curl}\,(\boldsymbol{u} \times \boldsymbol{\Omega}), \tag{6}$$

which shows the balance between the time-dependent and convection terms. Using $|\boldsymbol{u}| \sim \omega l$,

$$a/l \sim 1. \tag{7}$$

The experimental result shown in figure 6 supports this argument of scaling.

Another Reynolds number including θ is introduced to express the data for three different values of θ. By using the two-dimensional polar coordinates (r, ϕ), the balance between the time-dependent and viscous terms is written as

$$\frac{\partial \Omega}{\partial t} \sim \nu \left\{ \frac{1}{r} \frac{\partial}{\partial r} \left(r \frac{\partial \Omega}{\partial r} \right) + \frac{1}{r^2} \frac{\partial^2 \Omega}{\partial \phi^2} \right\}. \tag{8}$$

The order estimation of this relation gives

$$\omega \sim \nu \left\{ \frac{1}{a^2} + \frac{1}{a^2 \theta^2} \right\}, \tag{9}$$

where $r \sim a$, $\partial/\partial r \sim 1/a$ and $\partial^2/\partial^2 \phi \sim 1/\theta^2$ have been used. When $\theta \ll 1$, (9) becomes

$$\frac{a}{l} \sim \left(\frac{\nu}{\omega l^2 \theta^2}\right)^{\frac{1}{2}} = Re_2^{-\frac{1}{2}}, \tag{10}$$

where $Re_2 = \omega l^2 \theta^2 / \nu$.

The data for a/l are plotted against Re_2 in figure 7; a/l for $\theta \ll 1$ is proportional to $Re_2^{-\frac{1}{2}}$ for $Re_2 \ll 30$ and becomes constant for larger values of Re_2. By recalling that at $\theta = 12°$ the critical value of Re_1 for steady to unsteady vortex transition is 2.0×10^3, the critical value of Re_2 becomes about 90. An empirical formula for a curve on which the data collapse is obtained by assuming $a/l = A + B\, Re_2^{-\frac{1}{2}}$ and applying the least-square fit method to determine the constants A and B. The result is

$$a/l = 0.321 + 5.55\, Re_2^{-\frac{1}{2}}, \tag{11}$$

which is drawn in figure 7 as a solid curve.

REFERENCES

HAGERTY, W. W. & MICH, A. A. 1950 Use of an optical property of glycerine–water solutions to study viscous fluid-flow problems. *Trans ASME* E: *J. Appl. Mech.* **17**, 54–58.

KANEKO, A. & HONJI, H. 1979 Double structures of steady streaming in the oscillatory viscous flow over a wavy wall. *J. Fluid Mech.* **93**, 727–736.

MATSUNAGA, N. & HONJI, H. 1980a The backwash vortex. *J. Fluid. Mech.* **99**, 813–815.

MATSUNAGA, N. & HONJI, H. 1980b Visualization of standing vortices behind a cylinder in glycerin–water solutions. *Rev. Sci. Instrum.* **51**, 314–316.